FULL PAPER

ADVANCED FUNCTIONAL MATERIALS

DOI: 10.1002/adfm.200700154

Influence of Molecular Dipoles on the Photoluminescence and Electroluminescence of Dipolar Spirobifluorenes**

By *Chih-Long Chiang*, *Shih-Min Tseng*, *Chin-Ti Chen*,* *Chao-Ping Hsu*,* and *Ching-Fong Shu**

This Full Paper investigates a series of strongly fluorescent donor–acceptor-substituted spirobifluorene compounds, red 2-diphenylamino-7-(2,2-dicyanovinyl)-9,9′-spirobifluorene (DCV), green 2-diphenylamino-9,9′-spirobifluorene7-carxoxaldehyde (CHO), and blue 2-diphenylamino-7-(2,2-diphenylvinyl)-9,9′-spirobifluorene (DPV), together with their spiro-linked "dimeric" analogs, 2DCV, 2,2′-bis(diphenylamino)-9,9′-spirobifluorene-7,7′-dicarboxaldehyde (2CHO), and 2,2′-bis(diphenylamino)-7,7′-bis(2,2-diphenylvinyl)-9,9′-spirobifluorene (2DPV), respectively. The emission optical density and, hence, the intensity of photoluminescence (PL) or electroluminescence (EL) of the "dimeric" analogs is presumed to increase, which is beneficial for organic light-emitting diode (OLED) applications. The physical properties, including the dipole moments obtained from quantum chemistry calculations, emission solvatochromism, fluorescence quantum yield (Φ_f) as well as the EL of these six spirobifluorene compounds have been examined in detail. We found that Φ_f as well as OLED performance (EL efficiency and intensity) of the strongly dipolar DCV decrease significantly in the "dimeric" analog 2DCV, but less so in the moderately dipolar CHO and 2CHO, and only slightly in the weakly dipolar DPV and 2DPV. This is parallel to the intramolecular dipole moment, which is large for 2DCV, medium for 2CHO, and very small for 2DPV. Here, we show for the first time systematically that the luminescence intensity is closely correlated with the local electric field induced by the molecular dipole. A strong electric field may facilitate radiationless decay channels with a charge-transfer nature, leading to a high quenching rate. Consistent with this conclusion, which is derived from the red DCV/2DCV and green CHO/2CHO, our new blue fluorophore DPV with an essentially zero dipole moment has successfully achieved one of the best electrofluorescent blue OLEDs. At the same time, by doping the highly dipolar DCV into an isolated environment with the low-polarity Alq_3 as the host matrix, we obtained a very high performance of saturated yellow OLEDs as well, This is possibly due to the reduction of emission-quenching dipoles from the neighboring molecules. Our results have provided an important insight in designing luminescent materials, as follows: molecular dipole moments should be kept at a low magnitude to avoid quenching induced by a strong local electric field in the chromophore.

1. Introduction

A general problem with using a fluorescent material in organic light-emitting diodes (OLEDs) and other luminescent devices is concentration quenching in the solid state.[1] Device engineers adopt a physical method, such as doping of the fluorescent material in an appropriate host, to alleviate the problem.[2] The success of such a physical method hinges on the molecular isolation and, hence, reduction of the molecular contact (π–π interaction) of the fluorophore in the solid state. A recently reported exception, a donor–acceptor-substituted spirobifluorene, 2-diphenylamino-7-(2,2-dicyanovinyl)-9,9′-spirobifluorene (DCV; Scheme 1) is one of those rare red fluorophores that is very efficient for non-dopant-based red OLEDs.[3] Based on the single-crystal X-ray structure, DCV has a unique molecular structure with a non-planar bulge π-framework, thereby avoiding π–π stacking between DCV molecules.

More recently we have synthesized a molecular "dimer" version of DCV, 2DCV (Scheme 1),[4] which has twice the chromophore density and offers the possibility to enhance photoluminescence (PL) or electroluminescence (EL). In fact, 2DCV performed much worse than did DCV in terms of EL intensity and efficiency.[5] In this paper, similar results have been found for "monomeric" 2-diphenylamino-9,9′-spirobifluorene7-carxoxaldehyde (CHO) when compared with "dimeric" 2CHO (Scheme 1). In contrast, newly prepared blue fluorophores 2-diphenylamino-7-(2,2-diphenylvinyl)-9,9′-spirobifluorene (DPV) and 2DPV (Scheme 1) performed rather similarly. The six molecules studied in the present work provide an ideal platform to study the factors influencing the luminescence yield, since each series of molecules is composed of a monomeric and

[*] Prof. C.-T. Chen, Prof. C.-P. Hsu, C.-L. Chiang, S.-M. Tseng
Institute of Chemistry
Academia Sinica
Taipei, Taiwan 11529 (R.O.C.)
E-mail: cchen@chem.sinica.edu.tw; cherri@chem.sinica.edu.tw
Prof. C.-F. Shu, C.-L. Chiang
Department of Applied Chemistry
National Chiao Tung University
Hsin-Chu, Taiwan 30050 (R.O.C.)
E-mail: shu@cc.nctu.edu.tw

[**] This work was supported by Academia Sinica and the National Science Council of Taiwan.

ADVANCED FUNCTIONAL MATERIALS

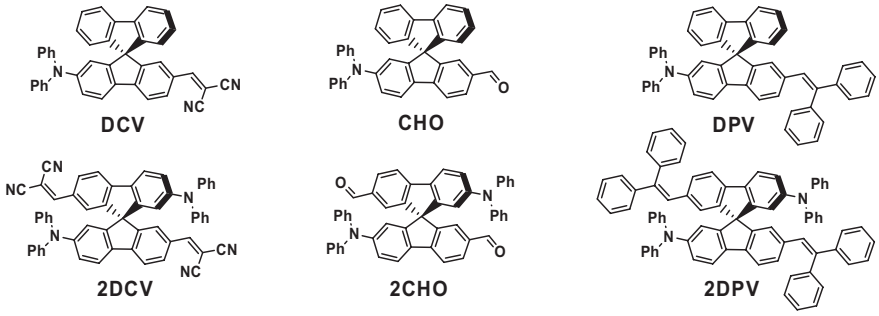

Scheme 1. Chemical structures of DCV, 2DCV, CHO, 2CHO, DPV, and 2DPV.

a dimeric pair and different series have a different dipolar character. The common bulky spirofluorene moiety can reduce the difference arising from intermolecular packing. We have demonstrated that the molecular dipole moment is a critical factor for the efficiency of luminescence, either PL or EL, taking examples of these spirobifluorene fluorophores. The molecular dipole from each molecular half of spirofluorenes gives rise to a strong local electric field and quenches PL or EL, possibly by making charge-transfer channels available. Therefore, we can define a new insight in understanding the performance of fluorescent materials, and derive new designing principles for OLED materials.

2. Results and Discussion

2.1. Photophysical Properties

Dimeric 2DCV possesses a very similar energy, both in absorption or emission wavelengths, to that of monomeric DCV (Table 1). This situation is similar in the green CHO/2CHO and blue DPV/2DPV pairs as well. This reflects the fact that an sp^3-hybridized carbon between the molecular halves of 2DCV, 2CHO, or 2DPV renders little electronic coupling (π-conjugated interaction).[6] At the same time, similar to other red dopant-based OLED materials, the color changes from red via orange to yellow (Fig. 1) with diminishing dopant concentration of DCV or 2DCV. This is commonly known as the solid-state solvation effect, induced by the doping molecules themselves.[2,7] It resembles the solvatochromism observed in the emission spectra, as shown in Table 1 and Figure 2. A red-shift is observed for solutions with solvents of increasing polarity. Such a phenomenon usually happens in molecules with a large change in its dipole when electronically excited, and with a large ground-state dipole that provides a polar environment in the solid state.[8] In addition, the bathochromic shifts of the emission from solution state to the condensed phase (solid state) were found to be varied for these spirobifluorene compounds: a very large shift for red DVC or 2DCV, a medium shift for green CHO or 2CHO, and virtually no shift for blue DPV or 2DPV (Table 1).

Such solvatochromism results imply that the molecular dipole moments of these three sets of spirobifluorene compounds (DCV/2DCV, CHO/2CHO, and DPV/2DPV) are substantially different from each other. Considering a rather similar transition energy of dimers of 2DCV, 2CHO, or 2DPV to the corresponding monomers, DCV, CHO, or DPV, respectively, it begs the question why the blue spirobifluorenes (DPV/2DPV) behave so differently from the green (CHO/2CHO) or red (DCV/2DCV) ones. Moreover, since the performance of OLEDs based on 2DPV and DPV is relatively similar, why does the performance of 2DCV and DCV OLEDs differ so much? We searched for an explanation based on the relatively large red-shift of the emission wavelength, which has a significantly smaller fluorescence quantum yield, as well as in the large difference in OLED performance of 2DCV or 2CHO. We found and verified that the key to the explanation is the ground-state molecular dipole moment of the dipolar spirobifluorene compounds, as detailed below.

Table 1. Optical properties and energy levels of spirobifluorene compounds

	Solution		Solid state	ΔE[c]	HOMO/LUMO
	λ_{max}^{ab},λ_{max}^{fl} [a] [nm,nm]	Φ_f [b] [%]	λ_{max}^{fl}, Φ_f [nm,%]	[eV]	[eV/eV]
DCV	460, 582	79,70,49	633, 33	2.41	5.73/3.32
2DCV	460, 587	31,14, 7	654, 6	2.39	5.75/3.36
CHO	400, 497	83,68,62	502, 42	2.83	5.61/2.78
2CHO	401, 495	49,46,30	508, 10	2.83	5.63/2.80
DPV	385, 468	60,60,56	467, 51	2.91	5.50/2.59
2DPV	385, 468	50,54,43	468, 21	2.89	5.53/2.64

[a] DPV and 2DPV were in chlorobenzene; CHO, 2CHO, DCV and 2DCV were in 1,4-dioxane. [b] In chlorobenzene, 1,4-dioxane, and ethyl acetate, respectively. [c] Band-gap energies estimated from the red edge of absorption spectra.

2.2. Molecular Dipole Moments

The molecular dipole moments of these six spirobifluorenes were estimated by density functional theory (DFT) calculations (Fig. 3). The red spirobifluorenes possess large molecular dipole moments (11–15 Debye) and those of the blue spirobifluorenes are very small (< 1 Debye), whereas those of green spirobifluorenes are in the middle range (5–7 Debye). This is consistent with the electron push–pull properties of the functional groups in the molecules. DCV has a strong electron withdrawing dicyanovinyl group, and in CHO, the formyl group has a medium strength of withdrawing π-electrons and, hence, there is a polarization effect in between the functionalties of dicyanovinyl and diphenylvinyl. Qualitatively, this agrees with the intermediate dipole moment calculated for CHO/2CHO compared with those of DVC/2DCV and DPV/2DPV. The ground-state dipole of 2DCV can be considered as a simple

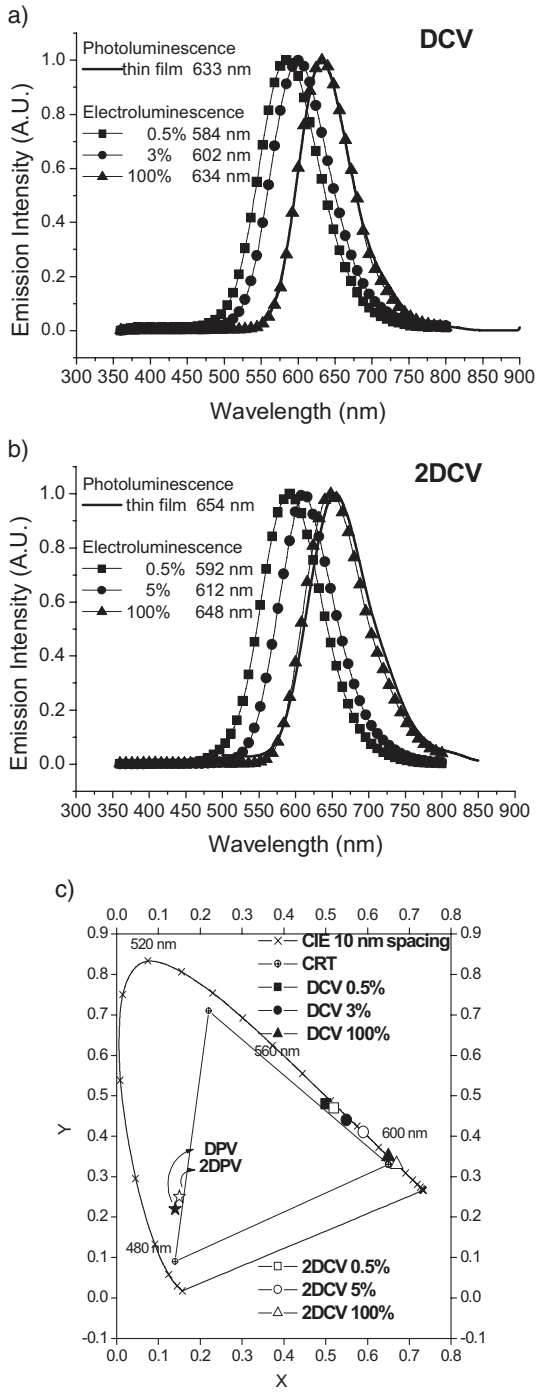

Figure 1. PL and EL spectra of OLEDs based on a) DCV, and b) 2DCV. The 1931 CIE (the Commission Internationale de l'Ecairage) color chromaticity diagram of all OLEDs, including those of DPV and 2DPV ones, are shown in (c).

vector sum of the two dipoles of the two orthogonally linked fragments. When the molecular dipole moment (10.59 Debye) of DCV was used to model the dipole of a half fragment in 2DCV, then a simple vector summation ($2 \times 10.59 \times \cos 45°$) leads to 14.95 Debye of 2DCV (Fig. 3, bottom), which is very close to 14.50 Debye obtained by the same calculation for 2DCV. A similar vector analysis of dipole moment works as well for 2CHO. Both DPV and 2DPV do not possess a electron-withdrawing functionality (the diphenylvinyl group is a very weak electron acceptor), and the calculated dipoles are not only small but also disoriented in a non-orthogonal direction (Fig. 4).

The calculated dipole moment differences between the ground state and the first excited state are much larger for DCV and 2DCV (6.14 and 4.43 Debye, respectively) than those for DPV and 2DPV (1.66 and 1.35 Debye, respectively). These dipole moment results are parallel to the solvatochromic behavior of these fluorescent spirobifluorenes in solution (see previous section of photophysical properties). The solvatochromism observed for spirobifluorene compounds is qualitatively in agreement with the dipole moment changes calculated for the red, green, and blue spirobifluorenes and following the known principle.[8,9] In solution, fluorescence quantum yields decrease as the solvent polarity increases (Table 1). Such solvent polarity dependence is particularly obvious in the case of the red pair of DCV/2DCV, is relatively less dependent for the green pair of CHO/2CHO, and is much less so in the case of the blue pair of DPV/2DPV (Table 1). Such behavior is also consistent with their relative dipole moment values, which are estimated by calculation.

2.3. PL/EL Quantum Yield, Molecular Dipole Moment, and Electric Field

Solution fluorescence quantum yields drop from monomeric to dimeric species, with a 60–85 % decrease for the red DVC→2DCV, 50–70 % for the green CHO→2CHO, and only a 10–25 % decrease for the blue DPV→2DPV (Table 1). The sensitivity of fluorescence quantum yields to the polarity in its surrounding implies that the polar environment may facilitate a non-radiative decay process leading to fluorescence quenching. This effect is closely related to a field-induced fluorescence quenching of donor–acceptor-substituted diphenyloligoene fluorophores reported earlier,[10] where an external electric field with a strength of ~ 1 MV cm^{-1} was applied to the fluorophore-doped polystyrene thin film. It was shown that under an external electric field, fluorescence quenching occurred on the fluorophore with large dipole moment changes between ground and the first excited states. Therefore, it was concluded that the external electric-field may lower the energy of a non-emissive intramolecular charge-transfer (ICT) state and become a quenching channel of the light emission.

We believe that the electric field, either external or local, has a strong influence on the spirobifluorene fluorophores in the OLEDs studied in this paper. Light-emitting materials experience an external electric field of 0.1–1.5 MV cm^{-1} (1–15 V applied to the device with ~ 100 nm thickness), which is comparable with those in Ref. [10]. Moreover, for dimeric donor–acceptor-substituted spirobifluorenes, the large ground state dipole moment may generate a local electric filed that has an even stronger effect on a nearby molecule or internally to the

ADVANCED FUNCTIONAL MATERIALS

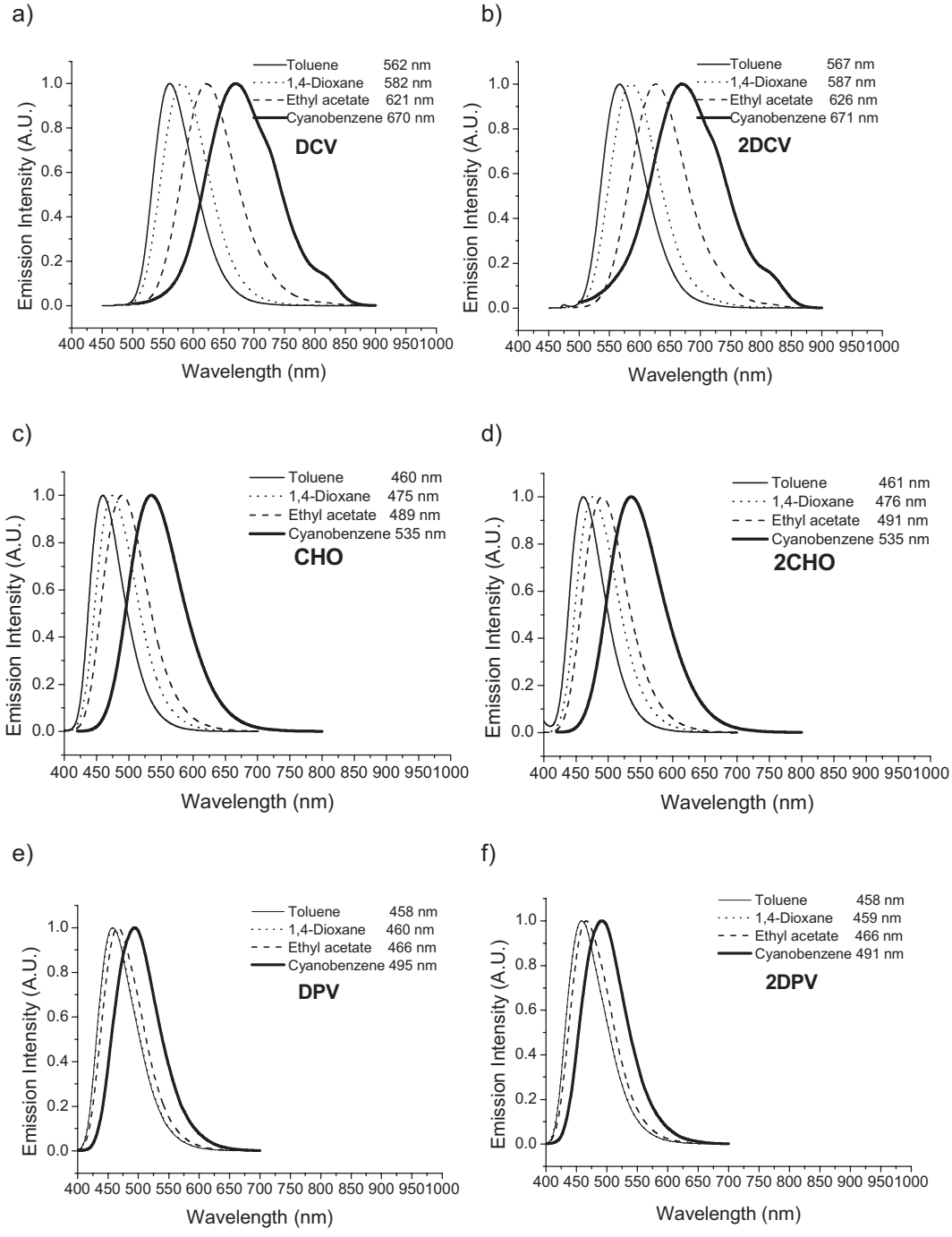

Figure 2. Fluorescence spectra of a) DCV, b) 2DCV, c) CHO, d) 2CHO, e) DPV, and f) 2DPV in toluene, 1,4-dioxane, ethyl acetate, and cyanobenzene, respectively.

other molecular half. The strength of the local electric field near a dipole moment can be estimated by

$$E = \frac{1}{4\pi\varepsilon_0 r^3}(3(\vec{\mu}\cdot\hat{r})\hat{r} - \vec{\mu}) \approx -\frac{\vec{\mu}}{4\pi\varepsilon_0 r^3} \quad (1)$$

where E is the electric field, $4\pi\varepsilon_0$ is 1.1×10^{-10} J^{-1} C^2 m^{-1}, r is the distance to the dipole, μ is the dipole moment in C m and 1 Debye = 3.34×10^{-30} C m. In Equation 1 we have used the field strength at the equatorial plane of the dipole as an estimate. For 2DCV, the edge-to-edge distance between the two molecular halves is about 5 Å.[3,5] Taking the calculated DFT value of 10 D for DCV as a model for the internal dipole moment of the monomer, each molecular half of 2DCV experiences a local electric field from the opposite half of the molecule with a strength of ~ 12 MV cm^{-1} (assuming half of a full charge separation), which is at least an order of magnitude

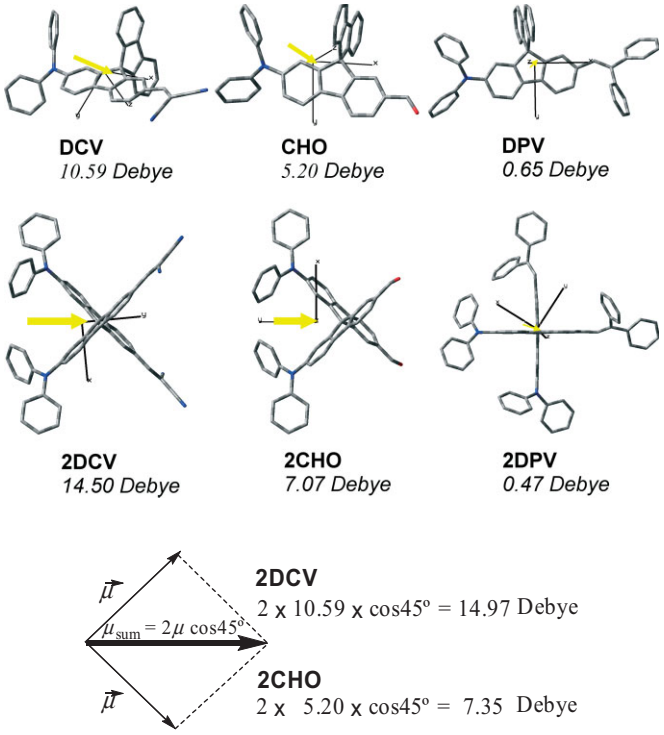

Figure 3. Dipole moments, in Debye (D), of DCV, CHO, DPV, 2DCV, 2CHO, and 2DPV obtained by DFT/B3LYP calculation. The direction and the approximate magnitude of the dipole are illustrated with a yellow arrow. Simple vector analysis of intramolecular dipoles and the net dipole moment of 2DCV and 2CHO is schematically presented in the bottom of the figure.

stronger than the external electric field of OLEDs and it can be very influential on the fluorescence quenching of the material. For the monomeric DCV, there is no intramolecular electric field but there is an intermolecular effect from the neighboring molecules, of which the strength of the electric field can be estimated to be as high as 12 MV/cm, assuming that the molecular separation distance is 5 Å. Such a value should be considered as an upper limit of the possible electric field because of the possible cancellation of all the surrounding molecular dipoles. Considering that the strength of such an electric field falls off quickly as the third power of distance from the molecules, dopant usage can significantly boost the performance of DCV OLEDs but not as much for 2DCV ones, as indicated in our data.

For nonpolar blue spirobifluorenes, the solution Φ_f of the blue 2DPV is only about 10–25 % smaller than that of DPV in solutions (Table 1), which is consistent with the very small dipole moments of both fluorophores, since they can not generate a local electric field with influential strength. The nonradiative decay resulting from the higher degree of vibrational motion of the floppy diphenylvinyl groups of 2DPV and DPV is likely to play a more significant role in fluorescence quenching than the effects of dipole moments herein.

2.4. Solid State Fluorescence Quantum Yield and Single Crystal X-Ray Structure

In the solid state, a big drop of fluorescence quantum yield from monomeric to dimeric spirobifluorenes was observed, ~ 82 % for red DCV→2DCV vs. ~ 59 % for blue DPV→2DPV. From the single-crystal X-ray data reported by us previously,[3,5] no intimate π-π contact was observed for DCV and 2DCV in the solid state, so we can mainly rule out the fluorescence quenching due to non-emissive excitons arising from π-π stacking. The drop of fluorescence quantum yield observed for blue DPV→2DPV is quite large, considering their very small dipole moment numbers. We can only surmise that it is the strong molecular contact of 2DPV in the solid state that leads to fluorescence quenching. Unfortunately, we did not have suit-

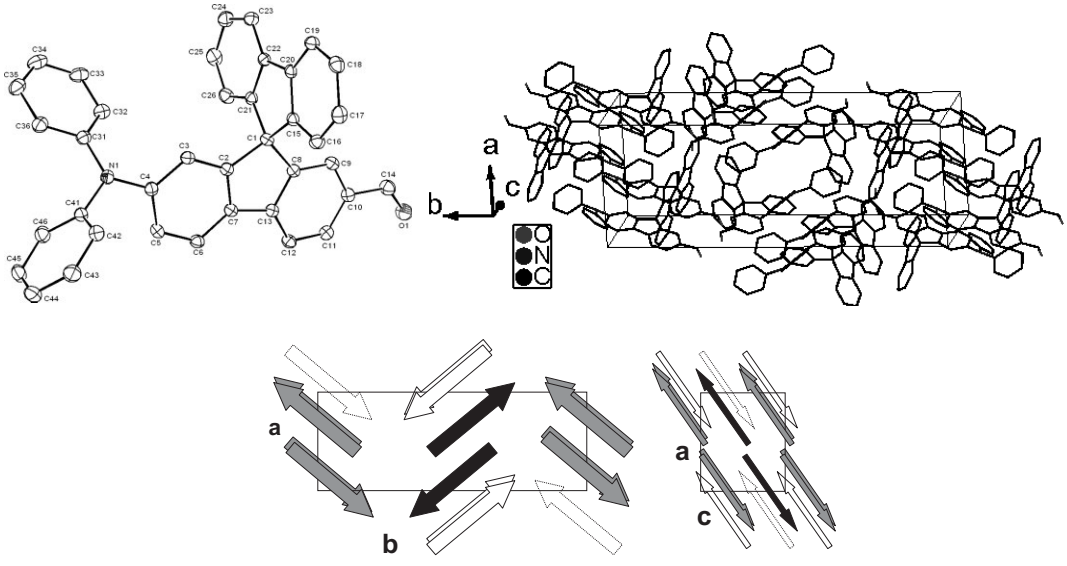

Figure 4. X-ray determined molecular structure and crystal packing diagram of CHO. The arrows in the packing diagram at the bottom indicate the direction from diphenylamino to formyl substituent. For clarity, molecules stacking in unit cells are marked with arrows having white, gray, or black shades.

ADVANCED FUNCTIONAL MATERIALS

able single crystals of DPV and 2DPV for X-ray crystallographic analysis to verify our conjecture. However, for green spirobifluorenes CHO→2CHO, a comparable ~ 76 % drop (with ~ 82 % drop of DCV→2DCV) of fluorescence quantum yield was observed as well. In that case, the drop of solid state fluorescence quantum yield could be attributed to the detrimental intermolecular π-π contact found for 2CHO (see the discussion of single crystal X-ray structure of CHO and 2CHO below).

The single crystals of **CHO** or **2CHO** were obtained from chloroform/dichloromethane/hexanes solution and were examined for X-ray diffraction structure analysis (see Figs. 4 and **5**).[11] There is no intermolecular face-on π–π interaction in CHO crystals. The intermolecular contacts are either non-orthogonal edge-to-face (C–H···π) or unparallel face-to-face π–π interaction, such as a 3.34 Å contact distance between C19 and C45, which is the contact between two nonparallel (~ 47°) benzene rings (Fig. 6 left) of fluorene and diphenylamino group. The closest contact found for the crystal of CHO is a 3.31 Å contact between the C34–C35 double bond and that of adjacent molecule. This is a short-distance contact but it is an edge-to-edge sideways interaction between two phenyl rings of neighboring molecules (Fig. 6 right), and it is unlikely to cause significant florescence quenching.

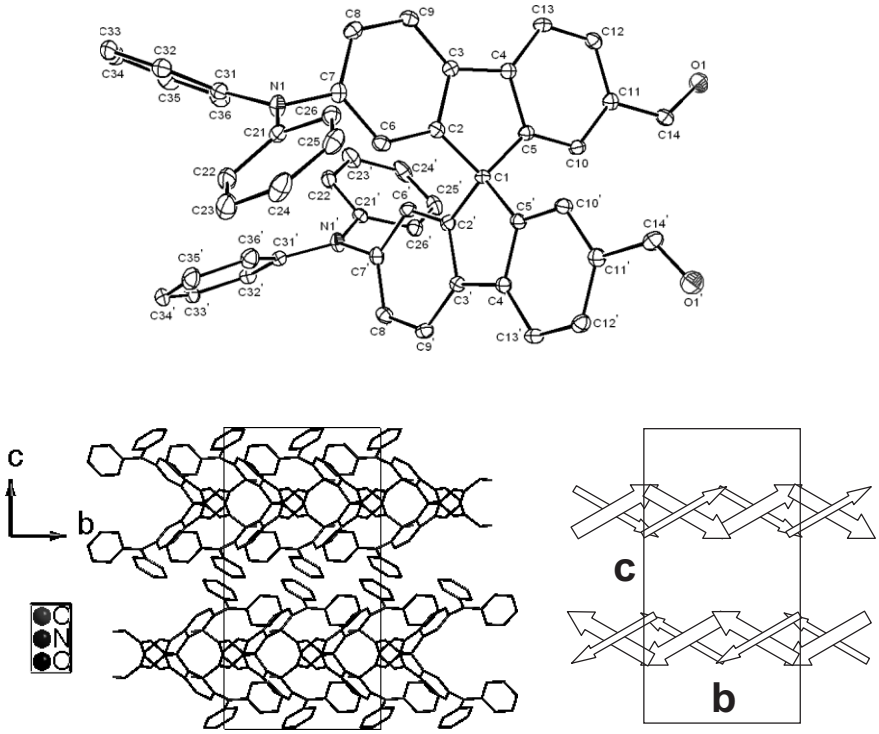

Figure 5. X-ray determined molecular structure and crystal packing diagram of 2CHO. The arrows in the packing diagram at the bottom indicate the direction from the diphenylamino to formyl substituent.

For the crystal structure of 2CHO, a direct face-on π-π interaction within the distance of ~ 3.4–3.5 Å was observed between the phenyl ring of the donor (diphenylamino group) and the C14–O1 double bond of the formyl acceptor of neighboring molecule (Fig. 7). Furthermore, because of the symmetry taking place in crystal packing, such face-on π–π interaction of 2CHO occurs twice for each molecule in the crystal. Therefore, a more significant fluorescence quenching can be expected for 2CHO than 2CHO in solid state. This deduction is consistent with the fact that 2CHO has about 40–50 % smaller Φ_fs than those of CHO in solution but nearly 75 % smaller Φ_fs in the solid state (Table 1)

2.5. OLEDs and High-Performance Yellow DCV Dopant and Blue DPV Non-Dopant

Figure 8 displays the characteristics of the devices, namely current density, voltage, external quantum efficiency, and electroluminance of all spirobifluorene OLEDs fabricated in the present research. Corresponding OLED data are summarized in the Experimental section.

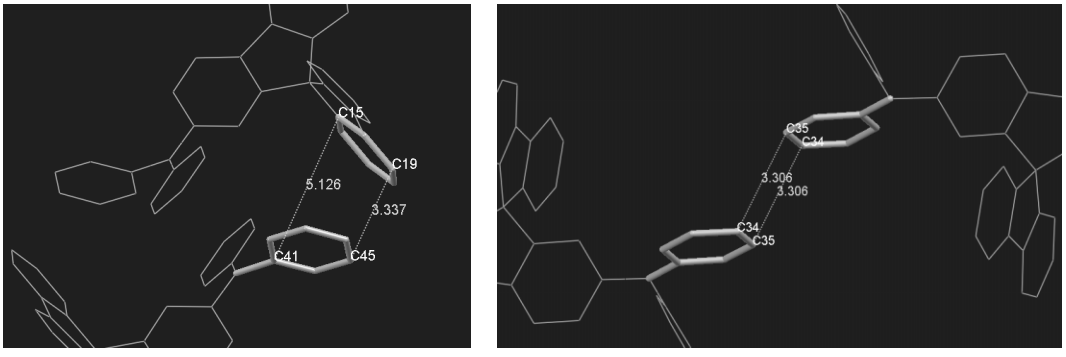

Figure 6. Left: an unparallel ring-to-ring contact between C19 and C45 (3.34 Å) of CHO. Right: an edge-to-edge sideways interaction between two phenyl rings of neighboring molecules of CHO.

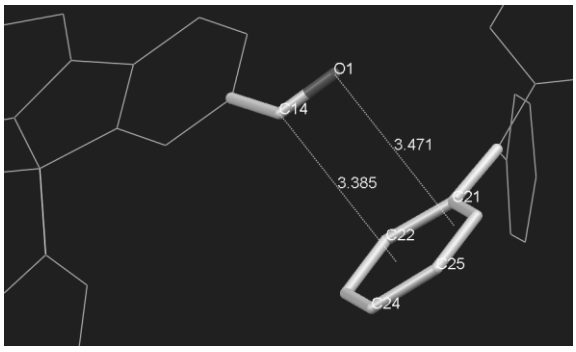

Figure 7. The face-on π–π interaction between formyl acceptor and the phenyl ring of diphenylamino donor of 2CHO.

Figure 9 illustrates the voltage dependency of external quantum efficiency and electroluminance. As mentioned earlier, dimeric 2DCV or 2CHO OLEDs performed much worse than the monomeric DCV or 2CHO OLEDs, whereas the performance of 2DPV OLEDs was just moderately inferior to that of DPV OLEDs. In addition, a typical roll-off of external quantum efficiency associated with the increase of applied voltage was observed for DCV/2DCV, CHO/2CHO, and DPV/2DPV OLEDs.

Consistent with this new insight derived from the red 2DCV and DCV, our new blue fluorophore DPV successfully achieved one of the best electrofluorescence blue OLEDs.[13] Non-dopant blue DPV OLEDs have outperformed other OLEDs with similar blue color purity ($CIE_{x,y}$ = 0.13–0.18, 0.16–0.24) in terms of EL efficiency and intensity: maximum efficiency of 3.4 %, 5.4 cd A^{-1}, or 5.7 lm W^{-1}, and the peak intensity of 33020 cd m^{-2} or 1430 cd m^{-2} at 20 mA cm^{-2} (Fig. 8 and Table 3). This can be ascribed to the practically zero dipole moment of DPV and, hence, few problems with electric-field-induced fluorescence quenching in the solid state. On the other hand, by doping the dipolar and bright **DCV** in an isolated environment (avoiding the effect of dipole moments from the neighbors), very high performance of saturated yellow OLEDs was obtained. Its EL efficiency is as high as 3.4 %, 9.4 cd A^{-1}, or 8.2 lm W^{-1}, and the peak EL intensity is 37640 cd m^{-2} and 1750 cd m^{-2} at 20 mA cm^{-2} (Fig. 8 and Table 3), which also outperforms most electrofluorescence yellow OLEDs.[14]

3. Conclusion

Owing to their unique structural feature, donor–acceptor-substituted spirobifluorenes including both monomeric and dimeric ones, provide an ideal model set in elucidating the influence of molecular dipole moment on fluorescence quenching in solution as well as in the solid state. EL and consequently the performance of OLEDs are strongly affected by the molecular dipole moment. In addition to the vibrational-motion-induced emission quenching and solid-state molecule–molecule contact quenching, which are well known sources of fluorescence quenching, the intramolecular and intermolecular electric field arising from the molecular dipoles is another detrimental factor that should be avoided in the molecular design of

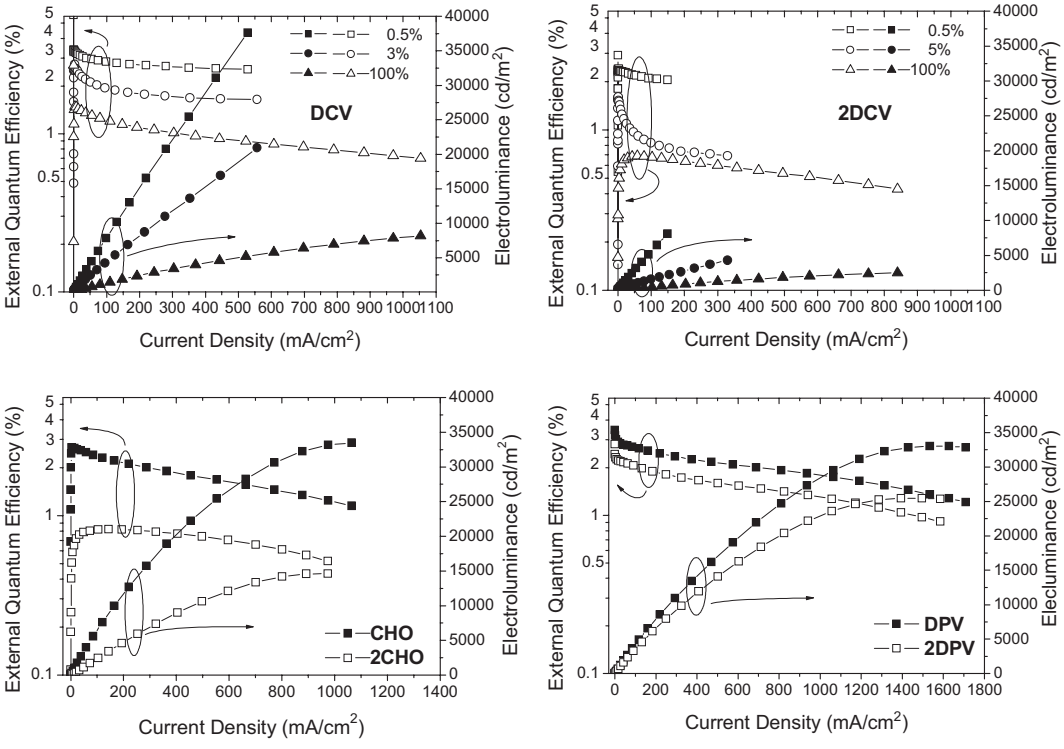

Figure 8. Electroluminescence characteristics (EL efficiency-current density-EL intensity) of OLEDs: ITO/NPB/DCV or 2DCV:Alq_3(0.5, 3, 5, or 100 %)/BCP/Alq_3/Mg:Ag; ITO/NPB/CHO or 2CHO/BCP/Alq_3/Mg:Ag and ITO/NPB/DPV or 2DPV/TPBI/LiF/Al [12].

ADVANCED FUNCTIONAL MATERIALS

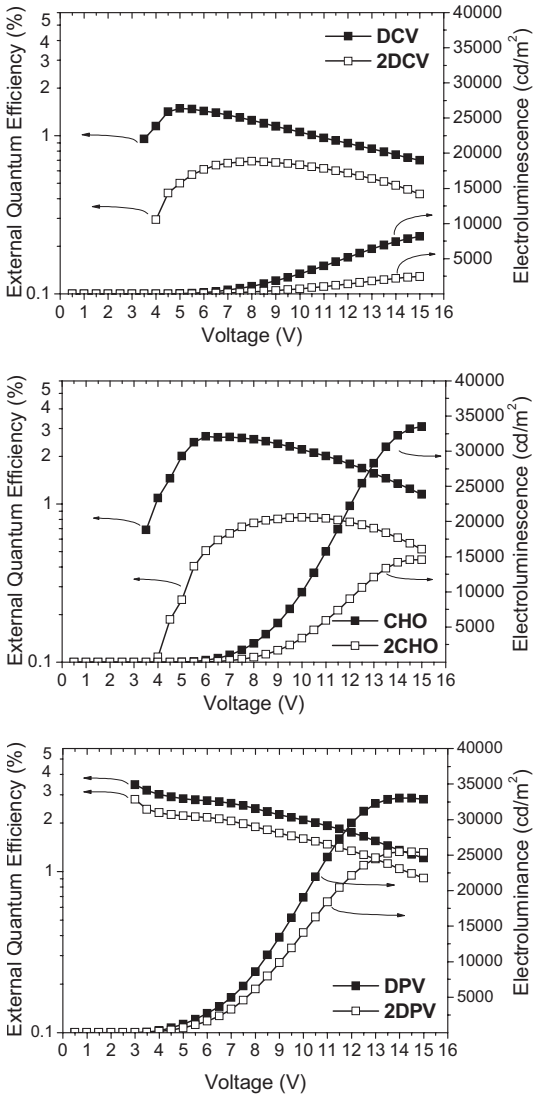

Figure 9. Electroluminescence characteristics (EL efficiency-voltage-EL intensity) of OLEDs: ITO/NPB/DCV or 2DCV/BCP/Alq_3/Mg:Ag, ITO/NPB/CHO or 2CHO/BCP/Alq_3/Mg:Ag, and ITO/NPB/DPV or 2DPV/TPBI/LiF/Al.

high performance fluorophores for OLEDs. This is quite a challenge for the red (or long-wavelength) light-emitting materials because most of the molecular structure of red fluorophore with an appreciable intensity of electrofluorescence are based on a donor–acceptor-substituted π-conjugated system and they are dipolar in nature.[1] Unlike dimeric 2DCV, the outstanding performance of a DCV-based non-dopant OLED is one rare exception. Only modest solid-state fluorescence quenching was found for DCV, and it is due to the bulky and rigid molecular framework of spirobifluorene that prevents the molecules from close contact and hence reduces the adverse π-π interaction as well as the strength of the intermolecular electric field.

From the dipole moment properties of these fluorescent materials, we arrived at a convincing explanation of why the dimeric DCV (or 2CHO) exhibit a significantly worse OLEDs performance than the monomeric DCV (or 2CHO) OLED. Consequently, in addition to the high performance of non-dopant red DCV OLEDs, we have successfully achieved one of the best electrofluorescent yellow OLEDs using DCV as dopant material. We have also achieved one of the best electrofluorescent blue OLEDs using an efficient and bright DPV non-dopant material that has a practically zero dipole moment and hence a very limited electric-field-induced fluorescence quenching in the solid state.

4. Experimental

General Methods: Both solution and solid-state fluorescence quantum yields (Φ_fs) of the donor–acceptor-substituted sprirobifluorenes were determined by the integrating-sphere method described by de Mello et al. [3,15]. The ionization potentials (or HOMO energy levels) of six spirobifluorene compounds were determined by low energy photo-electron spectrometry (Riken-Keiki AC-2). From our previous data, we found that the precision of the AC-2 measurement is about ±0.05 eV. LUMO energy levels were estimated by subtracting the energy gap (ΔE) from the HOMO energy levels. ΔE was determined by the on-set absorption energy from the absorption spectra of the materials.

Materials: The synthesis and characterization of DCV, 2DCV, CHO, 2CHO, and 2DPV have been reported previously [3,4]. Blue fluorophore DPV was previously unknown and the details of the synthesis are reported in the present paper. Other materials involved in the fabrication of dopant or non-dopant OLEDs, tris(9-hydroxyquinoline)aluminum (Alq_3), 1,4-bis(1-naphylphenylamino)biphenyl (NPB), 2,2′,2″-(1,3,5-phenylene)-tris[1-phenyl-1*H*-benzimidazole] (TPBI) were prepared in the laboratory using published methods and were subjected to gradient sublimation prior to use. Hole-blocking material, 2,9-dimethyl-4,7-diphenyl-1,10-phenanthroline, bathocuproine (BCP), was purchased from Aldrich and used as received.

*Synthesis of 2-Diphenylamino-7-(2,2-diphenylvinyl)-9,9′-spirobifluorene (**DPV**)*: Under a nitrogen atmosphere, NaH (0.26 g, 60 wt % in oil, 6.20 mmol) was added to a diethoxydiphenylmethylphosphonate (1.88 g, 6.02 mmol) dry THF solution (10 mL), and the mixture was stirred for 1 h at 55 °C. After cooling, CHO (1.50 g, 2.93 mmol) was added, then the reaction solution was heated to refluxing temperature for 16 h. After cooling to room temperature, the reaction mixture was added to water, extracted with ethyl acetate, and dried over $MgSO_4$. The solution was concentrated under reduced pressure and subjected to flash column chromatography (silica gel, dichloromethane/hexanes: 1/5). A yellow solid was obtained with a yield of 88 % (1.7 g). ^{1}H NMR (400 MHz, $CDCl_3$, δ): 7.66 (d, 2H, J = 7.6 Hz), 7.57 (d, 1H, J = 8.3 Hz), 7.49 (d, 1H, J = 8.0 Hz), 7.29 (td, 2H, J = 7.5 Hz, J = 0.9 Hz), 7.17-7.22 (m, 5H), 6.97–7.11 (m, 11H), 6.92–6.97 (m, 3H), 6.85–6.97 (m, 6H), 6.78 (s, 1H), 6.71 (d, 1H, J = 7.6 Hz), 6.48 (d, 1H, J = 2.0 Hz), 6.11 (s, 1H). ^{13}C NMR (125 MHz, $CDCl_3$, δ): 150.3, 148.6, 148.4, 147.5, 147.4, 143.2, 141.9, 141.5, 140.0, 139.9, 136.5, 136.2, 129.8, 129.4, 129.0, 128.3, 128.1, 127.5, 127.4, 127.3, 127.2, 124.8, 124.0, 123.8, 122.5, 120.5, 119.9, 118.8, 65.6. FAB-MS: calcd 661.8, m/z = 661.3 (M^+). Anal. calcd for $C_{51}H_{35}N$: C 92.35, H 5.49, N 2.49; found: C 92.55, H 5.33, N 2.12.

Theoretical Calculation: For theoretical dipole moment (μ) calculation, donor–acceptor-substituted spirobifluorene molecules were optimized by applying DFT with the hybrid B3LYP functional [16] and 6-31G* basis set. With the optimized structure, we calculated the ground state dipole moments with the Hartree-Fock (HF), DFT (B3LYP) models and the 6-31G* basis set. Excited state dipole moments were calculated using Configuration Interaction Singles (CIS)/6-31G*. In all cases the first excited states were highly optically active, as indicated by the large oscillator strengths (> 0.9). Therefore we used the first CIS excited state to model the observed light-emitting states. We avoided using time-dependent DFT because of its problem in describing states with a charge-transfer (CT) nature [17], which may arise from the donor–acceptor moieties and because such CT states

might interfere with the optically active states we investigated. Even though the CIS results might be less accurate than TDDFT, the qualitative trends in the CIS results can still offer correct physical insights. The results of the calculation are summarized in Table 2. All calculations were preformed with a developmental version of Q-Chem [18].

X-Ray Crystallography Studies: Data collection was carried out on a Bruker X8APEX CCD diffractometer at 100 K for CHO and 2CHO single crystals. Mo radiation ($\lambda = 0.71073$ Å) was used for both crystals. The unit cell parameters were obtained by a least-square fit to the automatically centered settings for reflections. Intensity data were collected by using the $\omega/2\theta$ scan mode. Corrections were made for Lorentz and polarization effects. The structures were solved by direct methods *SHELX-97* [19]. All non-hydrogen atoms were located from the difference Fourier maps and were refined by full-matrix least-squares procedures. Hydrogen atoms were calculated and refined with an overall isotropic temperature factor. Calculations and full-matrix least-squares refinements were performed utilizing the *WINGX* program package [20] in the evaluation of values of R (F_o) for reflections with $I > 2\sigma(I)$ and R_w (F_o), where $R = \Sigma||F_o| - |F_c||/\Sigma|F_o|$ and $R_w = [\Sigma\{w(F_o^2 - F_c^2)^2\}/\Sigma\{w(F_o^2)^2\}]^{1/2}$. Intensities were corrected for absorption.

Table 2. Calculated ground state dipole moments and differences in permanent dipole moments of the first excited state and ground state [a].

	Ground state dipole		First excited state dipole	Difference dipole moment
	μ_{gr}^{DFT}	μ_{gr}^{HF}	μ_{ex}^{CIS}	$\lvert\mu_{ex}^{CIS} - \mu_{gr}^{HF}\rvert$
DCV	10.59	10.40	16.50	6.14
CHO	5.20	5.10	9.56	4.46
DPV	0.65	0.46	2.07	1.66
2DCV	14.50	14.05	18.41	4.43
2CHO	7.07	6.79	9.97	3.13
2DPV	0.47	0.42	1.75	1.35

[a] in Debye. B3LYP/6-31G* and HF/6-31G* were used for ground state, and CIS/6-31G* for excited state calculations.

OLED Fabrication and EL Characterization: The fabrication of OLEDs and their EL characterization have been described elsewhere [13b]. The current, voltage, and light intensity (*I–V–L*) measurements were made simultaneously using a Keithley 2400 programmable source meter and a Newport 1835C Optical meter equipped with a Newport 818-ST silicon photodiode. The device was placed close to the photodiode such that all the forward light went to the photodiode. The effective size of the emitting diode was 3.14 mm^2, which is significantly smaller than the active area of the photodiode detector, a condition known as "under filling" to satisfy the measurement protocol [21]. Only light emitting from the front face of the devices was collected and used in subsequent calculations of external quantum efficiency according to the method described earlier [21]. The luminous flux (lm) has been defined previously [22], and we adopted it to meet the purpose of our research. EL characteristics of OLEDs are summarized in Table 3.

Energy-Level of Spirobifluorenes and their OLED Layer Structure Analysis: Together with other materials adopted in the OLED fabrication, the relative energy-level alignments and layer thickness of OLEDs are schematically depicted in Scheme 2 [23]. Since the HOMO energy levels of DCV/2DCV or CHO/2CHO are rather close (0.2–0.3 eV difference) to that of electron-transporting Alq_3 in OLEDs, a hole blocking layer of BCP was deployed in either DCV/2DCV or CHO/2CHO OLEDs to prevent the charge-recombination occurring on Alq_3 that emits undesired green light. A large energy gap (~ 0.8 eV difference) between the LUMO levels of NPB and DCV or CHO (2DCV or 2CHO) can effectively confine the electrons inside the light-emitting layer of CHO or DCV (2DCV or 2CHO) and facilitates charge recombination that leads to the EL of dopant or non-dopant OLEDs. Within this context, the same device configuration, except for a thinner NPB layer (5 nm), was adopted for the fabrication of non-dopant CHO and 2CHO OLEDs (bottom left scheme of Scheme 2). In order to enhance the performance of OLEDs, blue DPV or 2DPV OLED was fabricated in different configuration: ITO/NPB(10 nm)/DPV or 2DPV (40 nm)/TPBI (50 nm)/LiF(1 nm)/Al (see the bottom right scheme of Scheme 2). There is no need of BCP here owing to the relatively large difference (~ 0.7 eV difference) of HOMO energy levels between TPBI and DPV (or 2DPV).

Table 3. Electroluminescence characteristics of dopant and non-dopant OLEDs of DCV, 2DCV, CHO, 2CHO, DPV, and 2DPV.

	Doping level of devices [wt. %]	Max. luminance and voltage [cd m^{-2}, V]	Luminance, Efficiency, Voltage [cd m^{-2}, %, V] [e]	Max. efficiency [%, cd A^{-1}, lm W^{-1}]	λ_{max}^{el} [nm]	CIE 1931 chromaticity [x, y]
DCV	0.5 [a]	37640, 15	1750,3.1, 9.1	3.4, 9.4, 8.2	584	0.50, 0.48
DCV	3 [a]	20950, 15	1080,2.4, 9.1	2.7, 6.3, 4.1	602	0.55, 0.44
DCV	100 [b]	8190, 15	3103,1.4,6.3	1.5, 1.6, 1.1	634	0.65, 0.35
2DCV	0.5 [a]	8080, 15	1210,2.3,11.3	2.4, 6.4, 4.5	592	0.52, 0.47
2DCV	5 [a]	4290, 15	430,1.2,9.1	1.6, 3.0, 2.3	612	0.59, 0.41
2DCV	100 [b]	2470, 15	90,0.66,6.6	0.69,0.47,0.22	648	0.67, 0.33
CHO	100 [c]	33470, 15	1430, 2.6, 7.3	2.7, 7.3, 3.8	502	0.19, 0.50
2CHO	100 [c]	14600, 15	410, 0.7, 7.5	0.8, 2.4, 0.9	506	0.20, 0.53
DPV	100 [d]	33020, 14	910,2.9,4.7	3.4,5.4, 5.7	478	0.14, 0.22
2DPV	100 [d]	25470, 15	780,2.2,5.1	2.8,4.9, 5.1	480	0.15, 0.25

[a] Devices have the configuration of ITO/NPB/DCV or 2DCV: Alq3/BCP/Alq3/Mg:Ag (top right diagram in Scheme 2). [b] ITO/NPB/DCV or 2DCV/BCP/Alq3/Mg:Ag (top left diagram in Scheme 2). [c] ITO/NPB/CHO or 2CHO/BCP/Alq3/Mg:Ag (bottom left diagram in Scheme 2). [d] Devices have the configuration of ITO/NPB/DPV or 2DPV/TPBI/LiF/Al (bottom right diagram in Scheme 2). [e] At current density of 20 mA cm^{-2}

Received: February 1, 2007
Revised: October 6, 2007

[1] C.-T. Chen, *Chem. Mater.* **2004**, *16*, 4389.
[2] a) C. W. Tang, S. A. VanSlyke, C. H. Chen, *J. Appl. Phys.* **1989**, *65*, 3610. b) V. Bulovic, A. Shoustikov, M. A. Baldo, E. Bose, V. G. Kozlov, M. E. Thompson, S. R. Forrest, *Chem. Phys. Lett.* **1998**, *287*, 455. c) C. H. Chen, J. Shi, C. W. Tang, *Macromol. Symp.* **1997**, *125*, 1.
[3] C.-L. Chiang, M.-F. Wu, D.-C. Dai, Y.-S. Wen, J.-K. Wang, C.-T. Chen, *Adv. Funct. Mater.* **2005**, *15*, 231.
[4] C.-L. Chiang, C.-F. Shu, C.-T. Chen, *Org. Lett.* **2005**, *7*, 3717.
[5] C.-L. Chiang, M.-F. Wu, C.-F. Shu, C.-T. Chen, *Proc. SPIE-Int. Soc. Opt. Eng.* **2005**, *5632*, 80.
[6] N. Johansson, D. A. dos Santos, S. Guo, J. Cornil, M. Fahlman, J. Salbeck, H. Schenk, H. Arwin, J. L. Brédas, W. R. Salanek, *J. Chem. Phys.* **1997**, *107*, 2542.
[7] V. Bulovic, R. Deshpande, M. E. Thompson, S. R. Forrest, *Chem. Phys. Lett.* **1999**, *308*, 317.
[8] Examples see: C. Reichardt, *Solvents and Solvent Effects in Organic Chemistry*, VCH, Weinheim **1988**.
[9] C.-T. Chen, S.-Y. Liao, K.-J. Lin, C.-H. Chen, T.-Y. J. Lin, *Inorg. Chem.* **1999**, *38*, 2734.
[10] T. Nakabayashi, Md. Wahadoszamen, N. Ohta, *J. Am. Chem. Soc.* **2005**, *127*, 7041.
[11] Crystal data for **CHO**: $C_{38}H_{25}NO$: $Fw = 511.59$, monoclinic, $P2_1/c$, $Z = 4$, $F(000) = 1072$. Cell dimensions: $a = 10.3824(2)$ Å, $b =$

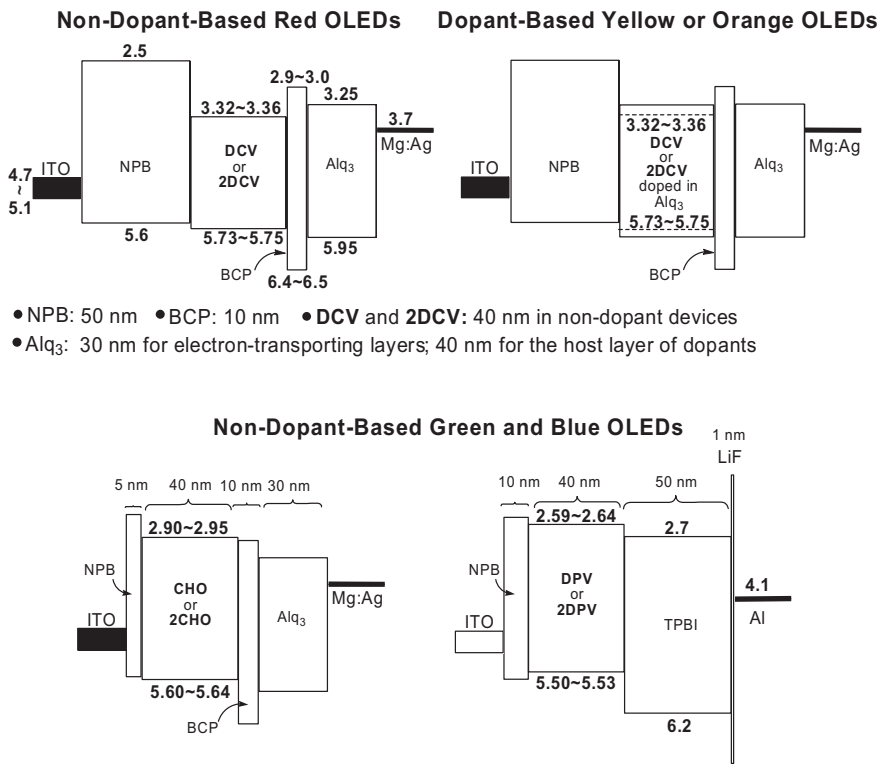

Scheme 2. Relative energy-level alignments and layer thickness of OLEDs.

28.2780(6) Å, c = 8.9198(2) Å, α = 90°, β = 91.7920(10)°, γ = 90°, V = 2617.51(10) Å^3, $2\theta_{max}$ = 50.0°, ρ_{calcd} = 1.298 g cm^{-3}. Of 20425 reflections, 4628 were independent, 362 parameters, R (F_o) = 0.0301 (for reflections with $I > 2\sigma(I)$), R_w (F_o) = 0.0640 (for reflections with $I > 2\sigma(I)$). The GoF on F^2 was equal 0.854. Crystal data for **2CHO**: $C_{51}H_{34}N_2O_2$: Fw = 706.80, orthorhombic, $Pbcn$, Z = 4, $F(000)$ = 1480. Cell dimensions: a = 14.9404(4) Å, b = 11.3117(3) Å, c = 21.3320(6) Å, α = 90°, β = 90°, γ = 90°, V = 3605.14(17) Å^3, $2\theta_{max}$ = 50.0°, ρ_{calcd} = 1.302 g cm^{-3}. Of 28706 reflections, 3017 were independent, 250 parameters, R (F_o) = 0.0395 (for reflections with $I > 2\sigma(I)$), R_w (F_o) = 0.0833 (for reflections with $I > 2\sigma(I)$). The GoF on F^2 was equal 0.925. CCDC-645601 and CCDC-645602 contain the supplementary crystallographic data of CHO and 2CHO, respectively. These data can be obtained free of charge via www.ccd.cam.ac.uk/conts/retrieving.html (or from the Cambridge Crystallographic Data Centre, 12, Union Road, Cambridge CB21EZ, UK; fax: (+44)1223-336-033; or deposit@ccdc.cam.ac.uk).

[12] The layer thickness of each OLED is described in Scheme 2 in the Experimental section.

[13] a) Y.-H. Kim, D.-C. Shin, S.-H. Kim, C.-H. Ko, H.-S. Yu, Y.S. Chae, S.-K. Kwon, *Adv. Mater.* **2001**, *13*, 1690. b) L.-H. Chan, R.-H. Lee, C.-F. Hsieh, H.-C. Yeh, C.-T. Chen, *J. Am. Chem. Soc.* **2002**, *124*, 6469. c) K. Danel, T.-H. Huang, J. T. Lin, Y.-T. Tao, C.-H. Chuen, *Chem. Mater.* **2002**, *14*, 3860. d) J. Shi, C. W. Tang, *Appl. Phys. Lett.* **2002**, *80*, 3201. e) M. Guan, Z. Q. Bian, Y. F. Zhou, F. Y. Li, Z. J. Li, C. H. Huang, *Chem. Commun.* **2003**, 2708. f) K. R. J. Thomas, J. T. Lin, Y.-T. Tao, C.-H. Chien, *Adv. Funct. Mater.* **2003**, *13*, 445. g) W.-J. Shen, R. Dodda, C.-C. Wu, F.-I. Wu, T.-H. Liu, H.-H. Chen, C. H. Chen, C.-F. Shu, *Chem. Mater.* **2004**, *16*, 930. h) C.-H. Chen, F.-I. Wu, C.-F. Shu, C.-H. Chien, Y.-T. Tao, *J. Mater. Chem.* **2004**, *14*, 1585. i) F.-I. Wu, C.-F. Shu, T.-T. Wang, E. W.-G. Diau, C.-H. Chien, C.-H. Chuen, Y.-T. Tao, *Synth. Met.* **2005**, *151*, 285. j) K. R. J. Thomas, M. Velusamy, J. T. Lin, C.-H. Chien, Y.-T. Tao, *J. Mater. Chem.* **2005**, *15*, 4453. k) J. Y. Shen, C. Y. Lee, T.-H. Huang, J. T. Lin, Y.-T. Tao, C.-H. Chien, C. Tsai, *J. Mater. Chem.* **2005**, *15*, 2455. l) F.-I. Wu, P.-I. Shih, M.-C. Yuan, A. K. Dixit, C.-F. Shu, Z.-M. Chung, E. W.-G. Diau, *J. Mater. Chem.* **2005**, *15*, 4753. m) S. Tao, Z. Peng, X. Zhang, P. Wang, C.-S. Lee, S.-T. Lee, *Adv. Funct. Mater.* **2005**, *15*, 1716. n) X. R. Wang, J. S. Chen, H. Yiou, D. G. Ma, R. G. Sun, *Jpn. J. Appl. Phys. Part 1* **2005**, *44*, 8480. o) R. J. Tseng, R. C. Chiechi, F. Wudl, Y. Yang, *Appl. Phys. Lett.* **2006**, *88*, 093512. p) C. Tang, F. Liu, Y.-J. Xia, J. Lin, L.-H. Xie, G.-Y. Zhong, Q.-L. Fan, W. Huang, *Org. Electron.* **2006**, *7*, 155. q) R. C. Chiechi, R. J. Tseng, F. Marchioni, Y. Yang, F. Wudl, *Adv. Mater.* **2006**, *18*, 325. r) H.-C. Li, Y.-P. Lin, P.-T. Chou, Y.-M. Cheng, R.-S. Liu, *Adv. Funct. Mater.* **2007**, *17*, 520. s) C. J. Tonzola, A. P. Kulkarni, A. P. Gifford, W. Kaminsky, S. A. Jenekhe, *Adv. Funct. Mater.* **2007**, *17*, 863.

[14] a) Z. Y. Xie, L. S. Hung, S. T. Lee, *Appl. Phys. Lett.* **2001**, *79*, 1048. b) X. Q. Lin, B. J. Chen, X. H. Zhang, C. S. Lee, H. L. Kwong, S. T. Lee, *Chem. Mater.* **2001**, *13*, 456. c) K. R. J. Thomas, J. T. Lin, Y.-T. Tao, C.-H. Chuen, *Chem. Mater.* **2002**, *14*, 2796. d) K. R. J. Thomas, J. T. Lin, Y.-T. Tao, C. H. Chuen, *J. Mater. Chem.* **2002**, *12*, 3516. e) K. R. J. Thomas, J. T. Lin, Y.-T. Tao, C. H. Chuen, *J. Mater. Chem.* **2002**, *12*, 3852. f) W.-F. Xie, C.-N. Li, S.-Y. Liu, *Chin. Phys. Lett.* **2003**, *20*, 956. g) T.-H. Liu, Y.-S. Wu, M.-T. Lee, H.-H.Chen, C.-H. Liao, C. H. Chen, *Appl. Phys. Lett.* **2004**, *85*, 4304. h) H.-Y.Chen, Chi, Y. C.-S. Liu, J.-K. Yu, Y.-M. Cheng, K.-S. Chen, P.-T. Chou, S.-M. Peng, G.-H. Lee, A. J. Carty, S.-J. Yeh, C.-T. Chen, *Adv. Mater.* **2005**, *17*, 567. i) F. Nüesch, D. Berner, E. Tutiš, M. Schaer, C. Ma, X. Wang, B. Zhang, L. Zuppiroli, *Adv. Funct. Mater.* **2005**, *15*, 323. j) J. Lee, Y.-Y. Yuan, Y. Kang, W.-L. Jia, Z.-H. Lu, S. Wang, *Adv. Funct. Mater.* **2006**, *16*, 681. k) Y.-S. Wu, T.-H. Liu, H.-H. Chen, C. H. Chen, *Thin Solid Films* **2006**, *496*, 626.

[15] J. C. de Mello, H. F.Wittmann, R. H. Friend, *Adv. Mater.* **1997**, *9*, 230.

[16] A. D. Becke, *J. Chem. Phys.* **1993**, *98*, 5648.

[17] A. Dreuw, M. Head-Gordon, *J. Am. Chem. Soc.* **2004**, *126*, 4007.

[18] J. Kong, C. A. White, A. I. Krylov, C. D. Sherrill, R. D. Adamson, T. R. Furlani, M. S. Lee, A. M. Lee, S. R. Gwaltney, T. R. Adams, C. Ochsenfeld, A. T. B. Gilbert, G. S. Kedziora, V. A. Rassolov, D. R. Maurice, N. Nair, Y. Shao, N. A. Besley, P. E. Maslen, J. P. Dombroski, H. Daschel, W. Zhang, P. P. Korambath, J. Baker, E. F. C. Byrd, T. Van Voorhis, M. Oumi, S. Hirata, C.-P. Hsu, N. Ishikawa, J. Florian, A. Warshel, B. G. Johnson, P. M. W. Gill, M. Head-Gordon, J. A. Pople, *J. Comput. Chem.* **2000**, *21*, 1532.

[19] G. M. Sheldrick, SHELXL-97, University of Göttingen, Germany **1997**.

[20] L. J. Farrugia, *J. Appl. Crystallogr.* **1999**, *32*, 837.

[21] S. R. Forrest, D. D. C. Bradley, M. E. Thompson, *Adv. Mater.* **2003**, *15*, 1043.

[22] G. Wyszecki, W. S. Stiles, *Color Science: Concepts and Methods, Quantitative Data and Formulae*, Wiley, New York, NY **1982**, p. 259.

[23] In this study, we estimated the HOMO energy level of the material by AC-2 measurement instead of cyclic voltammetry (CV). This is because the samples subjected to the measurement are in solid state for AC-2 rather than in solution for CV. Solid-state samples are consistent with the form in OLEDs. It is well-known now that the solution CV-determined HOMO energy levels are different from those determined by solid-state photoemission spectroscopy, such as AC-2. B. W. D'Andrare, S. Datta, S. R. Forrest, P. Djurovich, E. Polikarpov, M. E. Thompson, *Org. Electron.* **2005**, *6*, 11.